Asymmetric caging in soft colloidal mixtures

C. MAYER[1,2]*, E. ZACCARELLI[1]*, E. STIAKAKIS[3†], C. N. LIKOS[2,4], F. SCIORTINO[1], A. MUNAM[5], M. GAUTHIER[5], N. HADJICHRISTIDIS[6], H. IATROU[6], P. TARTAGLIA[7], H. LÖWEN[2] AND D. VLASSOPOULOS[3,8]

[1]Dipartimento di Fisica and CNR-INFM-SOFT, Università di Roma La Sapienza, I-00185 Rome, Italy
[2]Institut für Theoretische Physik II: Weiche Materie, Heinrich-Heine-Universität, D-40225 Düsseldorf, Germany
[3]FO.R.T.H., Institute of Electronic Structure and Laser, GR-71110 Heraklion, Crete, Greece
[4]The Erwin Schrödinger International Institute for Mathematical Physics (ESI), Boltzmanngasse 9, A-1040 Vienna, Austria
[5]Department of Chemistry, Institute for Polymer Research, University of Waterloo, ON, N2L 3G1, Canada
[6]University of Athens, Department of Chemistry, GR-15771 Athens, Greece
[7]Dipartimento di Fisica and CNR-INFM-SMC, Università di Roma La Sapienza, I-00185 Rome, Italy
[8]University of Crete, Department of Materials Science and Technology, GR-71003 Heraklion, Crete, Greece
[†]Present address: Forschungszentrum Jülich, Weiche Materie, D-52425 Jülich, Germany
*e-mail: mayer@thphy.uni-duesseldorf.de; emanuela.zaccarelli@phys.uniroma1.it

Published online: 14 September 2008; doi:10.1038/nmat2286

The long-standing observations that different amorphous materials exhibit a pronounced enhancement of viscosity and eventually vitrify on compression or cooling continue to fascinate and challenge scientists[1], on the ground of their physical origin and practical implications. Glass formation is a generic phenomenon, observed in physically quite distinct systems that encompass hard and soft particles. It is believed that a common underlying scenario[2,3], namely cage formation, drives dynamical arrest, especially at high concentrations. Here, we identify a novel, asymmetric glassy state in soft colloidal mixtures, which is characterized by strongly anisotropically distorted cages, bearing similarities to those of hard-sphere glasses under shear. The anisotropy is induced by the presence of soft additives. This phenomenon seems to be generic to soft colloids and its origins lie in the penetrability of the constituent particles. The resulting phase diagram for mixtures of soft particles is clearly distinct from that of hard-sphere mixtures and brings forward a rich variety of vitrified states that delineate an ergodic lake in the parameter space spanned by the size ratio between the two components and by the concentration of the additives. Thus, a new route opens for the rational design of soft particles with desired tunable rheological properties.

Colloidal hard spheres, a model system in which vitrification has been intensively studied, undergo a transition to a dynamically arrested state, that is, a glass[4], when their volume fraction exceeds a value of about 0.58. The glass formation is discussed in the context of caging[5]: owing to crowding, a given particle is trapped by its nearest neighbours in a virtual cage, schematically represented in Fig. 1a. Its macroscopic motion is significantly hindered, whereas fast local motions within the cage (rattling) are still possible[6]. Mode coupling theory (MCT) has been particularly successful in providing a first-principles description of this effect[7,8]. Another ideal model system to investigate the general features of glass formation is provided by star polymers, as they enable tuning of the softness of their interaction[9]. They consist of f chains chemically anchored on a common centre. The variation of the functionality f enables the realization and control of the softness. The glass formation of soft star polymers can also be formulated in the context of caging[10], as shown in Fig. 1a.

When dealing with two-component mixtures of hard/soft bodies, it is already known that multiple mechanisms of vitrification and melting scenarios are possible, leading, for example, to the formation of attractive glasses for colloid–polymer mixtures[11,12] or double glasses for hard-sphere ones[13], the existence of the former resting on a depletion picture, whereas that of the latter on geometry-driven caging of both components. Soft mixtures have much more in store, as we show here. Our study examines the variety of glassy states and the intricate vitrification and melting scenarios present in star polymer mixtures. We demonstrate that a novel form of arrested matter exists, which is characterized by the formation of strongly anisotropic randomly oriented cages with a low coordination number for the larger component, the smaller one undertaking the role of filling up the rest of the large-star cage that has been opened up. This asymmetric glass has no counterpart in hard colloidal mixtures, in which cage deformation has only been reported in the presence of shear[14,15].

We consider star polymer mixtures that are asymmetric both in functionality and in size, focusing on the addition of smaller stars to a dense solution of larger ones, which, in the absence of the additives, is vitrified. We recently established the existence of two glassy states in such binary star mixtures[16]. The two glassy states identified there were a single glass formed by the large stars, in which the small ones remained ergodic, diffusing through the voids of the vitrified matrix, and a double glass, in which both components were arrested. The former occurs for large size asymmetries and the latter for moderate to small ones. Both glasses were observed to melt on increasing the concentration of additives. Indeed, the addition of small stars strikingly leads to a restoration of ergodicity[16]. Here, we establish that, on further increase in small-star concentration, a new type of glass appears, which is uniquely distinguished from the other ones by means of various structural and rheological characteristics: it is a double, asymmetric glass, in which both components are arrested but the cages are strongly anisotropically deformed, the localization length being significantly smaller than in the original double glass.

Experimental evidence for the aforementioned re-entrant vitrification is provided in Fig. 1b. This figure shows the experimental kinetic phase (state) diagram for three different

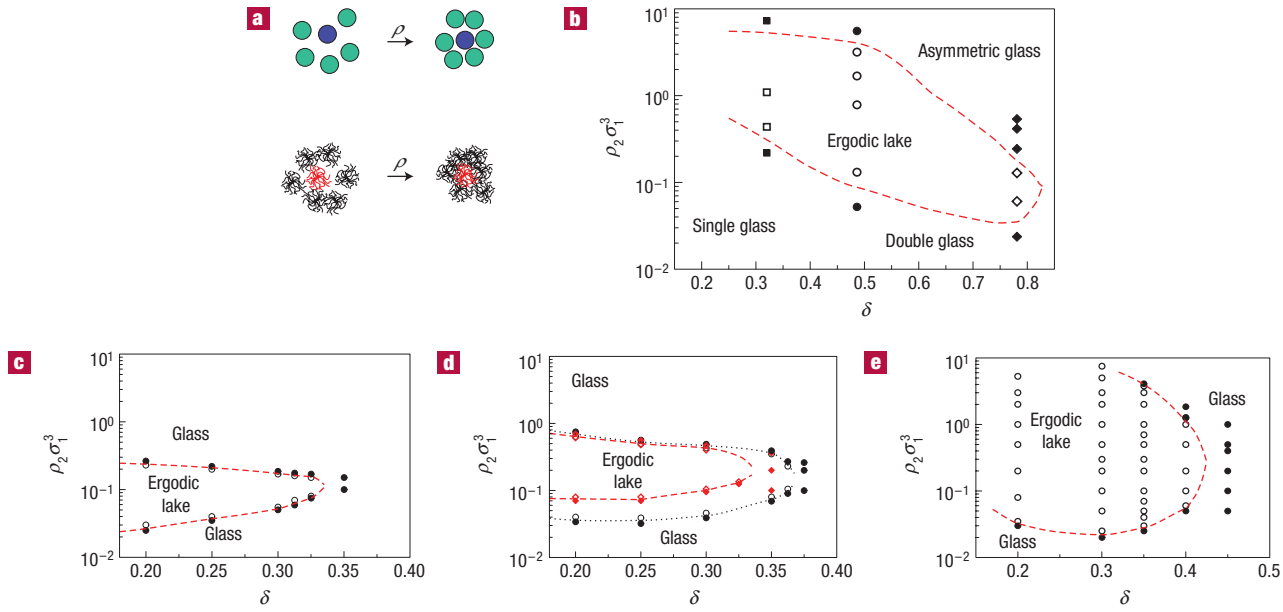

Figure 1 Experimental and MCT arrested state diagrams for star–star mixtures. a, Schematic representation of cages for hard spheres (top) and star polymers (bottom). **b–e**, Kinetic state diagrams in the plane spanned by size ratio δ and the additive number density $\rho_2\sigma_1^3$. Open symbols correspond to rheological fluids, filled symbols to rheological glasses. Dashed lines are guides to the eye to separate fluid from glassy states. **b**, Experimental results for different combinations of parameters: squares ($f_1 = 170$, $f_2 = 150$; $\rho_1\sigma_1^3 = 0.429$); circles ($f_1 = 128$, $f_2 = 141$; $\rho_1\sigma_1^3 = 0.477$); diamonds ($f_1 = 128$, $f_2 = 362$; $\rho_1\sigma_1^3 = 0.477$). **c**, MCT results for $f_1 = 128$, $f_2 = 141$ and $\rho_1\sigma_1^3 = 0.388$. **d**, MCT results for $f_1 = 170$ and $f_2 = 150$ for two different values of $\rho_1\sigma_1^3$ (0.358, circles; 0.36 diamonds). **e**, MCT results for $f_1 = 263$, $f_2 = 64$ and $\rho_1\sigma_1^3 = 0.345$.

studied mixtures (see Supplementary Information for materials and methods), drawn in the plane spanned by small/large star size ratio δ and the reduced number density of small stars $\rho_2\sigma_1^3$, where σ_1 is the corona diameter of the large stars. The density of the large stars is fixed so that, in the absence of additives, the system is vitrified. The mixture is also characterized by the functionalities f_1 and f_2 of the large and small stars, respectively. The experimental data show a 'lake' of ergodic fluid nested between various arrested states, found both for low and for high values of ρ_2. As sample availability prohibits us from making a full scan of the parameter space for one fixed combination f_1/f_2, we carry out MCT (ref. 17) and molecular dynamics simulations, which enable us to explore the dependence of the results on the values of the parameters. Interestingly, re-entrance is also observed in MCT calculations of the glass line, based on the emergence of a finite non-ergodicity parameter. Results for three different combinations of f_1 and f_2, encompassing the experimentally studied cases, are shown in Fig. 1c–e. Theory indicates that the presence of an ergodic region is a generic feature of star–star mixtures and rather insensitive to the precise f_1/f_2 values. Moreover, the extension of the ergodic region can also be tuned by changing either the functionalities of the two components or the density of the large stars, as shown in Fig. 1d.

Dynamic rheological data are shown in Fig. 2a for three state points of the same mixture at a low (1), intermediate (2) and large (3) density of additives, demonstrating the transitions from solid to fluid, and to solid again, on increasing ρ_2. The corresponding plateau moduli G' in the solid phase are reported in Fig. 2b, normalized with respect to the value of the large-star glass plateau modulus G'_0 in the absence of additives. The figure also shows results of the corresponding MCT calculations. Both experimental and theoretical results show that the high-ρ_2 glass is characterized by an elastic modulus that may exceed that of the low-ρ_2 glass by up to an order of magnitude. The fact that the high-ρ_2 glass has a larger modulus can be explained in terms of its smaller localization length l_0, following the proposition that the modulus relates to maximum excursion of a caged particle of radius R as[18] $G' = k_B T/(l_0^2 R)$. Our simulations (see below) confirm this picture.

We carry out extensive molecular dynamics simulations, and from the long-time limit of the mean-squared displacement (MSD), we calculate the isodiffusivity curves[12] for the large stars in the (δ, ρ_2) plane, reported for one specific set of parameters in Fig. 3a. These curves, evaluated in the ergodic region, are precursors of the glass line. Consistently with the experimental and MCT state diagrams, the isodiffusivity lines form an almost closed loop, confirming the existence of an ergodic lake in soft mixtures. Note that the left upper corner (small δ, large ρ_2) cannot be investigated neither in simulation nor in MCT owing to the presence of phase separation. Results for different parameters, reported in Supplementary Information, further stress the generality of this finding. The MSD also provides a way of estimating the localization length of the nearby glassy state. Indeed, the MSD exhibits a transient regime in between the short-time microscopic dynamics and the long-time diffusive behaviours. This transient regime marks the crossover between intra-cage and inter-cage dynamics. Therefore, the inflection point of the MSD versus time in a log–log scale provides a measure of the squared localization length l_0^2 for the stars. Figure 3b,c shows the MSD for two states, at low and high ρ_2 respectively, sufficiently close to the nearby glass transitions. On increasing ρ_2, l_0^2 decreases by roughly one order of magnitude, the same amount by which the elastic modulus G' increases (Fig. 2).

To gain insight into the nature of the arrested states, we focus on a constant-δ path that drives us from the low-ρ_2 double glass[16]

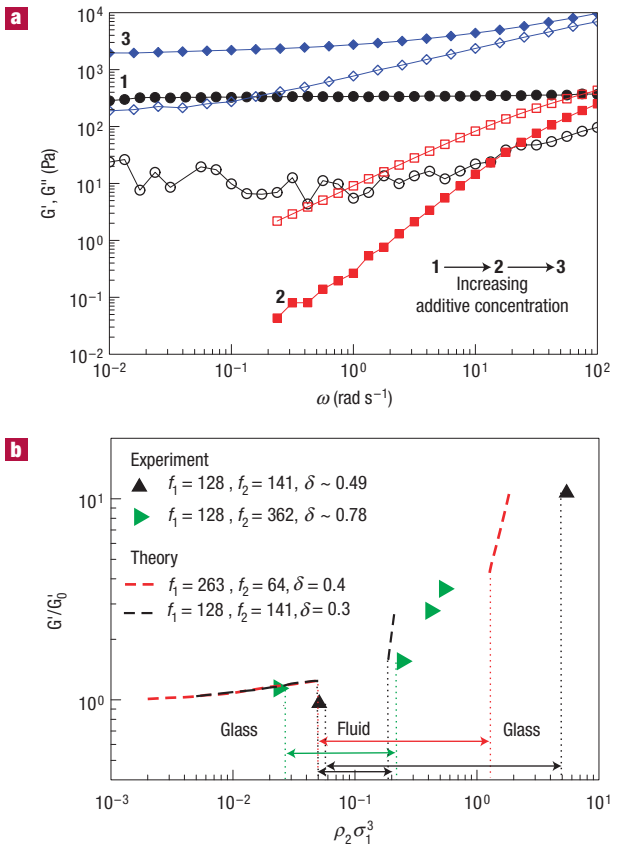

Figure 2 Rheological properties for star–star mixtures from experiments and MCT calculations. a, Dynamic frequency sweeps showing the storage G' (filled symbols) and loss G'' (open symbols) moduli as a function of oscillatory frequency ω (estimated at 0.1 rad s^{-1}) for a mixture consisting of large stars with $f_1 = 128$ at $\rho_1\sigma_1^3 = 0.477$ and small stars with $f_2 = 141$ at three different small-star densities (labelled as **1**, **2**, **3**): $\rho_2\sigma_1^3 = 0$ (black circles—glass); $\rho_2\sigma_1^3 = 0.78$ (red squares—fluid); $\rho_2\sigma_1^3 = 5.55$ (blue diamonds—glass). **b**, Ratio of G'/G_0', where G_0' is the storage modulus of the large-star system without additives, from experiments and MCT as a function of $\rho_2\sigma_1^3$. The vertical lines indicate the glass–fluid–glass transitions, with the horizontal arrows showing the corresponding fluid regions.

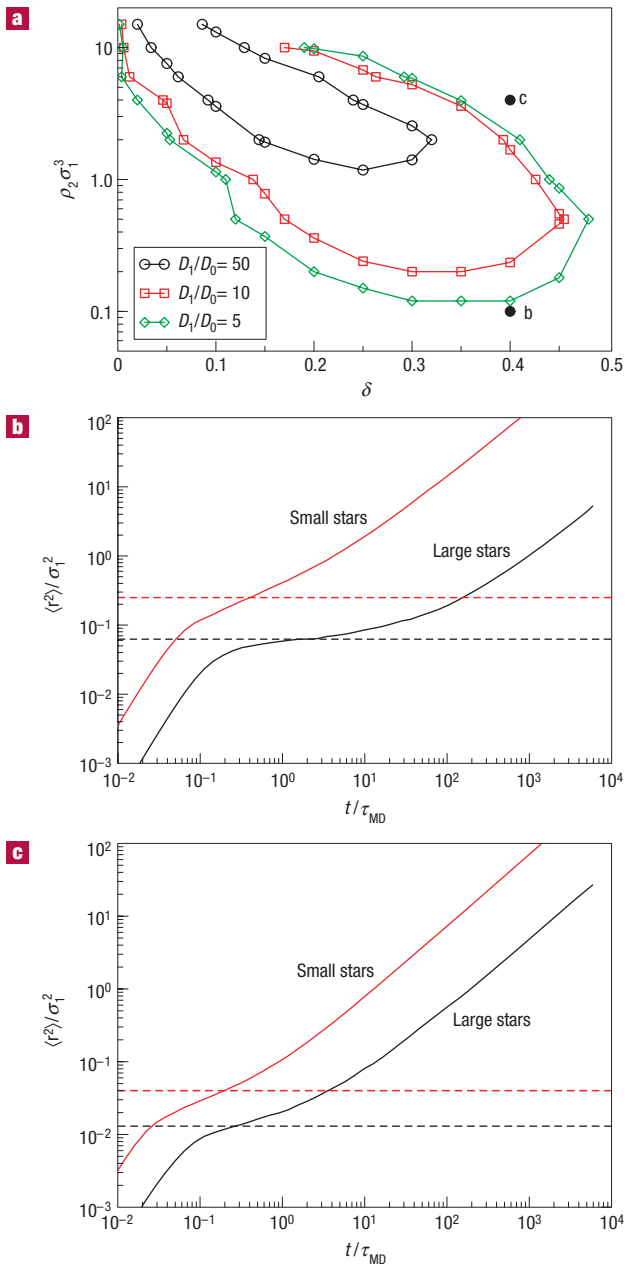

Figure 3 Dynamical properties of star–star mixtures based on numerical simulations. a, Isodiffusivity lines from simulations for $f_1 = 263$, $f_2 = 64$ and fixed $\rho_1\sigma_1^3 = 0.40$. The curves refer to three values of D_1/D_0, where D_1 is the self-diffusion coefficient of the large stars at the investigated state points, whereas D_0 is the corresponding one in the absence of additives. The two filled symbols denote the state points for which the dynamics are presented in **b** and **c**. **b**, MSDs of large and small stars close to the double glass (for $\rho_1\sigma_1^3 = 0.40$ and $\rho_2\sigma_1^3 = 0.1$). **c**, The same as in **b** but close to the asymmetric glass (for $\rho_1\sigma_1^3 = 0.40$ and $\rho_2\sigma_1^3 = 4.0$). Dashed lines in **b** and **c** indicate the (squared) localization lengths for the small and large particles.

to the high-ρ_2 novel glass through the ergodic fluid. The evolution of the liquid structure on addition of small stars is monitored by considering the large-star partial radial distribution functions $g_{11}(r)$. As observed in Fig. 4a, $g_{11}(r)$ clearly shows that large stars get pushed closer to each other as the density of small stars grows. More importantly, extra layering of the large stars appears, set by the length scale of the small ones. Indeed, the typical separation between the first and second peak becomes compatible with the size of the small stars when ρ_2 increases. This is clear evidence that the small stars are intervening between the large ones, drastically affecting their correlations. The structural rearrangement arises from the fact that the cross-interaction favours contacts between dissimilar species over large–large contacts. Thus, large stars tend to be separated by an increasing number of small stars as ρ_2 increases. We note that, oppositely to the depletion mechanism, a sufficiently high size ratio is necessary to cause these effects. Indeed, for $\delta = 0.1$ no significant structural changes are induced by the additives, as can be seen in Supplementary Information. On the other hand, for $\delta = 0.4$, the change of structure is associated with a spectacular drop in the coordination number of the large stars N_{11}: it decreases monotonically from about 13 to 3 as the density of additives grows. The observed monotonic decrease of coordination is a genuine effect, because the number density of large stars does not change.

The structural changes taking place on addition of small stars can be quantified by studying the configurations of typical

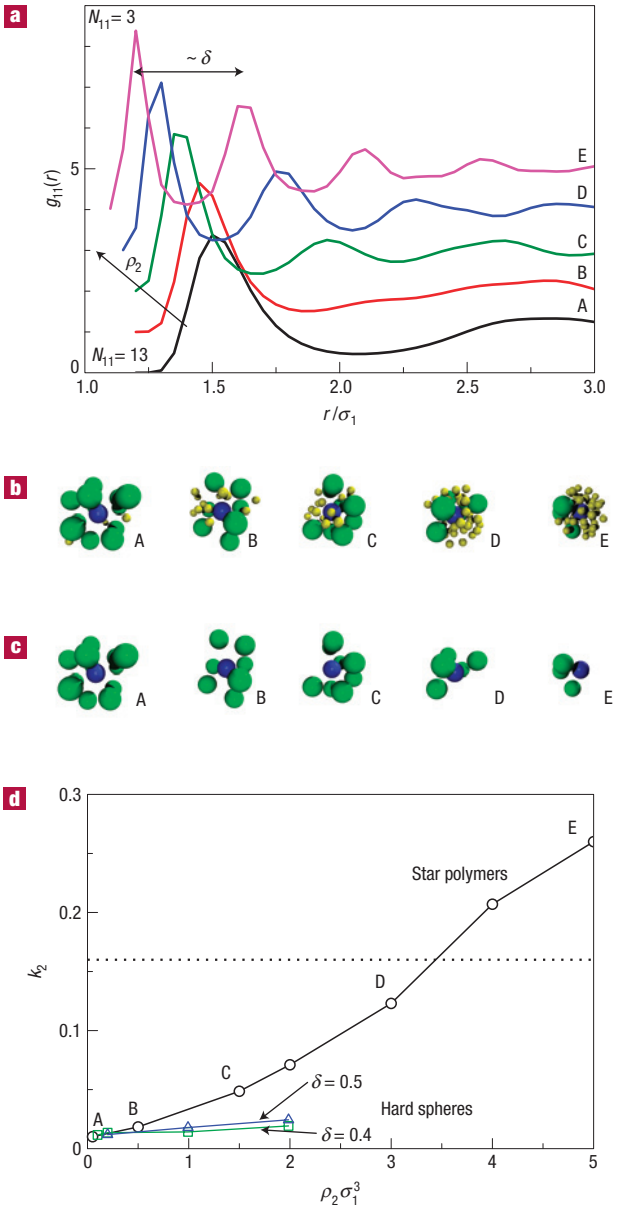

Figure 4 Structural properties of star–star mixtures and visualization of the asymmetric cages, based on numerical simulations. a, Radial distribution function of the large $f_1 = 263$ stars (progressively shifted by one along the *y* axis for clarity) at fixed $\rho_1\sigma_1^3 = 0.345$ in the presence of smaller $f_2 = 64$ stars ($\delta = 0.4$) for several values of $\rho_2\sigma_1^3$ (A: 0.05; B: 0.5; C: 1.5; D: 3; E: 5). **b**, Snapshots of the typical cages around a fixed large star (blue sphere) formed by neighbouring large (green spheres) and small (yellow spheres) stars in the studied state points A, B, C, D, E. Spheres are drawn with the appropriate particle size ratio. A cage surrounding a given large particle is defined by all stars (both large and small) within a distance corresponding to the first minimum of $g_{11}(r)$. **c**, Same as **b** but only large stars are shown. Note the pronounced decrease in the number of nearest neighbours for fixed large-star density: the cage volume shrinks as the peak of $g_{11}(r)$ moves to smaller r values as small stars are added. **d**, Anisotropy parameter k_2 as a function of ρ_2. The horizontal dotted line indicates the value corresponding to a regular planar configuration. **d** also shows k_2 for two hard-sphere mixtures with $\delta = 0.4$ and 0.5 and with $\rho_1\sigma_1^3 = 0.993$ for several values of $\rho_2\sigma_1^3$, encompassing the region where the thermodynamically stable crystal is AB_2 (ref. 23). For hard spheres, it is difficult to increase the density of small spheres beyond two, as the total packing fraction is already quite high.

cages of nearest neighbours of a large star as a function of the amount of additives. The cage geometry closely follows that of the first coordination shell of the underlying (supercooled) fluid. The geometry and composition of the caging particles around the reference central particle are found to change drastically as a result of increasing ρ_2. This is shown in Fig. 4b, where typical cages obtained from simulation snapshots for some studied values of ρ_2 are shown. The visualization of only the large stars, shown in Fig. 4c, facilitates the identification of the progressive development of asymmetric caging. For low additive concentrations, cages have a very high, spherical symmetry, typical of dense solutions of repulsive, spherosymmetric particles. However, for higher values of ρ_2, the cages open up (see, for example, configuration *C*) and become increasingly and strongly aspherical. As the number of large nearest neighbours also drops, it becomes impossible to form cages with spherical symmetry. The cage structure tends to become almost planar (~3 neighbours). The small stars fill up the empty space opened up by the expulsion of large stars from the first coordination shell, so that they actually deform the spherical cages, introducing a local anisotropy in the large-star configurations. Such anisotropy is uniquely random, as opposed to correlated anisotropy, which is induced by shearing of, for example, colloidal, hard-sphere systems[14,15].

A quantitative measure of the anisotropy and cage asymmetry in the mixture is provided by the moment of inertia tensor I of the large nearest neighbours of a selected large star. In particular, here we report the behaviour of the anisotropy parameter k_2, which depends only on rotational invariants of the inertia tensor (see Supplementary Information for materials and methods). Indeed, a configuration with spherical symmetry leads to $k_2 = 0$ whereas a linear arrangement approaches $k_2 = 1$. Between these two values, any regular planar arrangement yields $k_2 = 5/32 \sim 0.16$. The evolution of k_2 with increasing ρ_2 is shown in Fig. 4d. The anisotropy parameter grows by a factor 20, yielding further strong evidence of the deformation and anisotropic nature of the cages. The value $k_2 = 0.26$, reached for the highest ρ_2 investigated, indicates a very high anisotropy on a local scale and points to structures that lack regularity (random, anisotropic caging). Clearly, such low-coordinated cages are not capable of sustaining local stresses; the small stars act as agents that both create the anisotropy and at the same time fill up the opened-up space and eventually lead to re-entrant structural arrest. We have repeated the same calculations for different system parameters observing that the anisotropy is enhanced by large asymmetries ($f_2 \ll f_1$) and by values of ρ_1 close to the one-component glass transition value, because this facilitates the deformability of the cages. We have also evaluated the anisotropy parameter for binary hard-sphere mixtures for size ratio $\delta = 0.4$ and 0.5 (see Fig. 4d) to provide evidence that asymmetric cages are not found in hard-sphere systems (for a detailed discussion, see Supplementary Information).

Soft colloidal particles are frequently encountered in large-scale and microfluidic processing applications in the industrial environment[19,20], but also in a variety of products such as cosmetics and pharmaceuticals[21,22], where the stability of particles is crucial. Control of the flow of such formulations is hence of foremost importance. Colloidal star polymers have emerged as an ideal tunable model system for implementing some of these ideas. Here, we have demonstrated the unique ability of obtaining different types of glass by taking advantage of the softness of the interaction potential in mixtures. In particular, we have identified a novel arrested state of matter, which originates from a pronounced rearrangement of the cage-forming nearest neighbours, and brings about low coordination and high anisotropy on the local scale. It emerges out of a double glass of large and small stars on increasing

the concentration of the small component and it is re-entrant, following an intervening ergodic fluid. The width of the fluid lake directly influences the rheological properties of the ergodic fluid, which range from those of a normal Newtonian liquid when the fluid lake is broad to highly viscoelastic ones, when it is narrow. At the same time, the soft mixtures at hand provide a means to tune the properties of the glass, as the asymmetric arrested state has elastic moduli exceeding those of one-component star-polymer glasses by one order of magnitude. Our results, which are generic to systems with soft repulsive interactions of entropic nature, underline the various possibilities for designing and controlling such hybrid soft composite materials and the related ample opportunities for tuning their rheology.

Received 27 May 2008; accepted 19 August 2008; published 14 September 2008.

References

1. Editorial. So much more to know. *Science* **309**, 78–102 (2005).
2. Angell, C. A. Formation of glasses from liquids and biopolymers. *Science* **267**, 1924–1935 (1995).
3. Liu, A. J. & Nagel, S. R. Nonlinear dynamics—Jamming is not just cool any more. *Nature* **6706**, 21–22 (1998).
4. Pusey, P. N. & van Megen, W. Phase behaviour of concentrated suspensions of nearly hard colloidal spheres. *Nature* **320**, 340–342 (1986).
5. Cohen, E. G. D. & de Schepper, I. M. Note on transport processes in dense colloidal suspensions. *J. Stat. Phys.* **63**, 241–248 (1991).
6. Weeks, E. R., Crocker, J. C., Levitt, A. C., Schofield, A. C. & Weitz, D. A. Three-dimensional direct imaging of structural relaxation near the colloidal glass transition. *Science* **287**, 627–631 (2000).
7. Barrat, J.-L., Götze, W. & Latz, A. The liquid-glass transition of the hard-sphere system. *J. Phys. Condens. Matter* **1**, 7163–7170 (1989).
8. Dawson, K. A. *et al.* Higher order glass transition singularities in colloidal systems. *Phys. Rev. E* **63**, 011401 (2001).
9. Grest, G. S., Fetters, L. J., Huang, J. S. & Richter, D. Star polymers: Experiment, theory, and simulation. *Adv. Chem. Phys.* **XCIV**, 67–163 (1996).
10. Vlassopoulos, D., Fytas, G., Pakula, T. & Roovers, J. Multiarm star polymers dynamics. *J. Phys. Condens. Matter* **13**, R855–R876 (2001).
11. Pham, K. N. *et al.* Multiple glassy states in a simple model system. *Science* **296**, 104–106 (2002).
12. Zaccarelli, E. *et al.* Confirmation of anomalous behaviour in short-ranged attractive colloids. *Phys. Rev. E* **66**, 041402 (2002).
13. Imhof, A. & Dhont, J. K. G. Experimental phase diagram of a binary colloidal hard-sphere mixture with a large size ratio. *Phys. Rev. Lett.* **75**, 1662–1665 (1995).
14. Vermant, J. & Solomon, M. J. Flow-induced structure in colloidal suspensions. *J. Phys. Condens. Matter* **17**, R187–R216 (2005).
15. Besseling, R., Weeks, E. R., Schofield, A. B. & Poon, W. C. K. Three-dimensional imaging of colloidal glasses under steady shear. *Phys. Rev. Lett.* **99**, 028301 (2007).
16. Zaccarelli, E. *et al.* Tailoring the flow of soft glasses by soft additives. *Phys. Rev. Lett.* **95**, 268301 (2005).
17. Götze, W. in *Liquids, Freezing and Glass Transition* (eds Hansen, J.-P., Levesque, D. & Zinn-Justin, J.) 287 (North-Holland, Amsterdam, 1991).
18. Cloitre, M., Borrega, R., Monti, F. & Leibler, L. Glassy dynamics and flow properties of soft colloidal pastes. *Phys. Rev. Lett.* **90**, 068303 (2003).
19. Cicuta, P. & Donald, A. M. Microrheology: A review of the method and applications. *Soft Matter* **3**, 1449–1455 (2007).
20. Duoss, E., Twardowski, M. & Lewis, J. A. Sol–gel inks for direct-write assembly of functional oxides. *Adv. Mater.* **19**, 3485–3489 (2007).
21. Widawski, G., Rawiso, M. & Francois, B. Self-organized honeycomb morphology of star-polymer polystyrene films. *Nature* **369**, 387–389 (1994).
22. Soppimath, K. S., Tan, D. C.-W. & Yang, Y.-Y. pH-triggered thermally responsive polymer core–shell nanoparticles for drug delivery. *Adv. Mater.* **17**, 318–323 (2005).
23. Cottin, X. & Monson, P. A. Substitutionally ordered solid solutions of hard spheres. *J. Chem. Phys.* **102**, 3354–3360 (1995).

Supplementary Information accompanies the paper at www.nature.com/naturematerials.

Acknowledgements

Helpful discussions with J. Roovers are gratefully acknowledged. This work has been supported by the Marie Curie Network on Dynamical Arrest of Soft Matter and Colloids MRTNCT-2003-504712, the NoE SoftComp NMP3-CT-2004-502235 and the DFG through the SFB TR6. C.M. acknowledges financial support by the Alexander von Humboldt Foundation.

Author information

Reprints and permission information is available online at http://npg.nature.com/reprintsandpermissions.
Correspondence and requests for materials should be addressed to C.M. or E.Z.